Electronic Supplementary Material (ESI) for Chemical Communications.

Supporting Information

Autologous Manganese Phosphates with Different Mn Sites for Electrocatalytic Water Oxidation

Shujiao Yang,[a] Shanhong Wan,[a] Fanfan Shang,[a] Dandan Chen,[a] Wei Zhang*[a] and Rui Cao*[a]

Key Laboratory of Applied Surface and Colloid Chemistry, Ministry of Education, School of Chemistry and Chemical Engineering, Shaanxi Normal University, Xi'an 710119, P. R. China.

*Corresponding authors. Emails: zw@snnu.edu.cn (W.Z.); ruicao@snnu.edu.cn (R.C.).

General materials

$MnCl_2·4H_2O$ (99.0%, Fuchen), $(NH4)_3PO_4·3H_2O$ (98.0%, Alfa), $NaH_2PO_4·2H_2O$ (99.99%, Alfa), $Na_2HPO_4·12H_2O$ (99.99%, Alfa), Nafion (5 wt%, DuPont) were acquired from commercial suppliers and used without further purification. Milli-Q water of 18.2 MΩ•cm was used in all experiments unless otherwise specifically stated.

Synthesis of materials

In a typical process, 2.58 mmol $MnCl_2·4H_2O$ and 0.91 mmol $(NH_4)_3PO_4·3H_2O$ were dissolved in 8 mL of water and stirred at room temperature for 2 hours. Then, the generated suspension was sealed in a 10 mL Teflon-lined stainless steel autoclave and heated at 200 °C for 6 h. The obtained manganese phosphate microparticles ($Mn_5(PO_4)_2(PO_3(OH))_2·4H_2O$) were collected by centrifugal washing with water three times and dried in drying oven at 60 °C. The obtained white solid was further heat treated to prepare manganese pyrophosphate ($Mn_2P_2O_7$) and anhydrous manganese phosphate ($Mn_3(PO_4)_2$) as electrocatalysts. $Mn_2P_2O_7$ was obtained by calcining at 400 °C for 3 hours in muffle furnace, and $Mn_3(PO_4)_2$ was obtained at 600 °C for 3 hours.

Physical characterizations

Powder X-ray diffraction (PXRD) data were obtained by Rigaku D/Max2550VB+/PC X-ray diffractometer at 40 kV and 100 mA using Cu Kα radiation (λ = 1.5406 Å). The scanning electron microscope (SEM) images were collected on a Hitachi SU8020 cold-emission field emission scanning electron microscope with 5 kV accelerating voltage. Thermo gravimetric analysis was put into practice by heating the dry solid powder sample at a speed of 5 °C/min under nitrogen flow at 100 mL/min over 25 °C to 800 °C in a TGA Instruments SDT Q600. Derivative thermo gravimetric (DTG) information was acquired based on the TGA data. X-ray photoelectron spectroscopy (XPS) analysis was performed on a Kratos AXIS ULTRA XPS analyzer

using monochromatic Al Kα (hν = 1486.6 eV) X-ray source. The surface area was obtained by BET method. The UV-Vis absorption spectra of the supernatant of solid samples electrolyzed in PP solution for 2 hours were detected in the range of 200-800 nm using Shimadzu UV 3600.

Electrochemical studies

The electrochemical experiments were carried out at room temperature using the Electrochemical Workstation of CH instrument (CHI 660E). Standard three electrode system was used for cyclic voltammetry (CV) and differential pulse voltammetry (DPV). Glass carbon (GC) (0.07 cm^2) electrode was used as working electrode, graphite rod as auxiliary electrode and saturated Ag/AgCl as reference electrode. Typically, 4 mg of samples and 30 μL of Nafion were added into 1 mL of water-ethanol solution at volume ratio of 2 : 1. The mixed solution was ultrasonically treated for 30 minutes to form a uniform slurry. Then, 6 μL of the sample was dropped on the effective working area of the glassy carbon electrode and dried at room temperature. The catalyst loading on the working electrode was 0.17 mg cm^{-2}. Cyclic voltammetry (CV), at a scan rate of 50 mV s^{-1}, were recorded in 0.05 M phosphate buffered saline (PBS) solution (pH = 7) with iR-compensation. DPV was carried out at the amplitude of 0.005 V with iR-compensation. Controlled potential electrolysis (CPE) was used to evaluate the stability of the catalyst under the same experimental setup without iR-compensation. TOF Calculation: TOF = j × A / 4 × F × n, where j is the measured geometrical current density at a given overpotential of 380 mV, A is the surface area of the electrode, the number 4 represents four electron transfer for per mole of O_2, F is the Faraday constant, and n is the number of moles of the effective Mn atom on the surface, determined from the total charge by integration of the Mn^{2+}/Mn^{3+} redox peak area in the cyclic voltammogram.

DFT calculation

Periodic plane-wave density functional theory (DFT) calculations were performed

using the Vienna ab initio simulation package (VASP).[1,2] The exchange-correlation was described by the spinpolarized revised Perdew-Burke-Ernzerhof (rPBE) method of the generalized gradient approximation (GGA) with a plane-wave kinetic cutoff energy of 500 eV.[3] The projector augmented wave (PAW) depicted non-spherical contributions to the core from the gradient corrections.[4–6] The long-range interaction was characterized by the DFT-D3 method of Grimme with zero dampings.[7] The optimized convergence threshold of internal forces and electronic relaxation was set to 0.02 eV/Å and 10^{-5} eV, respectively. A 5*5*5 (bulk model) Monkhorst-pack grid sampled the Brillouin zone with a smearing broadening of 0.2 eV. We added 15 Å of vacuum perpendicular to the slab to avoid any spurious interaction with periodic images. Dipole correction perpendicular to the surface was applied. The distortion index is calculated by the following equation:

$$\Delta = \frac{1}{N}\sum_{k=1}^{N}\frac{|d_k - d_{\mathrm{m}}|}{d_{\mathrm{m}}}$$

where d_k and d_m are individual Mn-O bond lengths and mean values, respectively, and N is the number of Mn-O bonds in one polyhedron.

Results:

Bulk	Average bond length	Distortion index
$Mn_2P_2O_7$	2.26316156424	0.0345683398205
$Mn_3(PO_4)_2$	2.19311506556	0.0264512201991

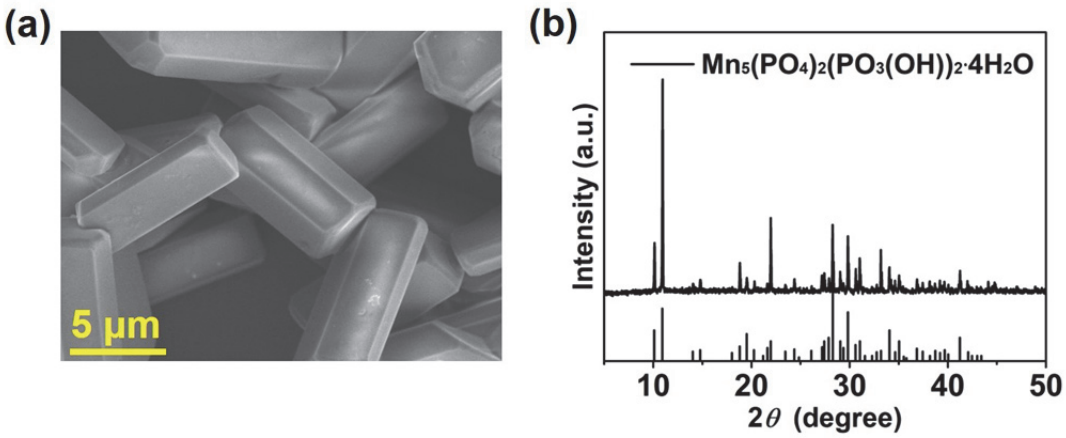

Fig. S1. (a) SEM and (b) XRD patterns of the as-prepared $Mn_5(PO_4)_2(PO_3(OH))_2{\cdot}4H_2O$.

<table>
<tr><td rowspan="9">$Mn_2P_2O_7$
 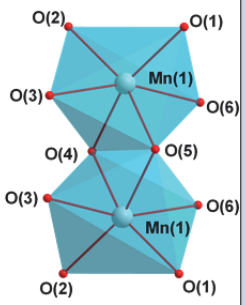

a=6.6330
b=8.5840
c=4.5460
β=102.67
C2/m</td><td rowspan="9">$Mn(1)O_6$</td><td>Atom</td><td>Bond (Å)</td><td>Atom</td><td>Angle (°)</td></tr>
<tr><td>Mn(1)-O(1)</td><td>2.132</td><td>O(1)-Mn(1)-O(6)</td><td>77.63</td></tr>
<tr><td>Mn(1)-O(2)</td><td>2.315</td><td>O(5)-Mn(1)-O(6)</td><td>84.55</td></tr>
<tr><td>Mn(1)-O(3)</td><td>2.164</td><td>O(4)-Mn(1)-O(5)</td><td>81.33</td></tr>
<tr><td>Mn(1)-O(4)</td><td>2.164</td><td>O(1)-Mn(1)-O(2)</td><td>98.62</td></tr>
<tr><td>Mn(1)-O(5)</td><td>2.315</td><td>O(2)-Mn(1)-O(4)</td><td>93.36</td></tr>
<tr><td>Mn(1)-O(6)</td><td>2.132</td><td>O(2)-Mn(1)-O(6)</td><td>115.37</td></tr>
<tr><td></td><td></td><td>O(3)-Mn(1)-O(5)</td><td>81.13</td></tr>
<tr><td></td><td></td><td>O(2)-Mn(1)-O(3)</td><td>77.63</td></tr>
<tr><td></td><td></td><td>O(1)-Mn(1)-O(5)</td><td>93.36</td></tr>
</table>

Fig S2. Crystal structure of Mn-polyhedrons, bond lengths and angle in $Mn_2P_2O_7$.

$Mn_3(PO_4)_2$

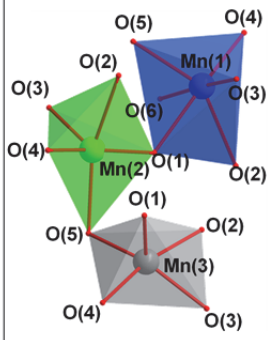

a=8.7994
b=11.4461
c=6.2506
β=98.97
$P2_1/c$

	Atom	Bond (Å)	Atom	Angle (°)
$Mn(1)O_6$	Mn(1)-O(4)	2.536	O(1)-Mn(1)-O(6)	79.97
	Mn(1)-O(3)	2.108	O(5)-Mn(1)-O(6)	80.42
	Mn(1)-O(2)	2.341	O(4)-Mn(1)-O(5)	102.48
	Mn(1)-O(1)	2.319	O(1)-Mn(1)-O(2)	62.15
	Mn(1)-O(5)	2.271	O(2)-Mn(1)-O(4)	106.48
	Mn(1)-O(6)	2.122	O(1)-Mn(1)-O(3)	92.88
$Mn(2)O_5$	Mn(2)-O(1)	2.003	O(1)-Mn(2)-O(5)	86.75
	Mn(2)-O(2)	2.356	O(1)-Mn(2)-O(2)	91.21
	Mn(2)-O(3)	2.086	O(1)-Mn(2)-O(3)	98.17
	Mn(2)-O(4)	2.016	O(3)-Mn(2)-O(4)	100.02
	Mn(2)-O(5)	2.272	O(2)-Mn(2)-O(4)	80.73
$Mn(3)O_5$	Mn(3)-O(1)	2.129	O(1)-Mn(3)-O(2)	108.19
	Mn(3)-O(2)	2.253	O(2)-Mn(3)-O(3)	74.37
	Mn(3)-O(3)	2.071	O(3)-Mn(3)-O(4)	94.97
	Mn(3)-O(4)	2.214	O(1)-Mn(3)-O(5)	104.21
	Mn(3)-O(5)	2.121	O(4)-Mn(3)-O(5)	100.91

Fig S3. Crystal structure of Mn-polyhedrons, bond lengths and angle in $Mn_3(PO_4)_2$.

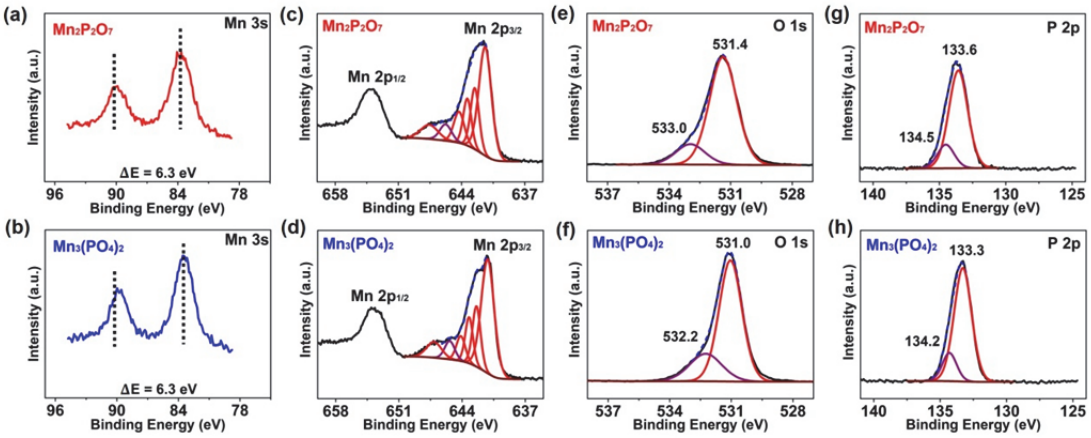

Fig S4. The XPS spectra of $Mn_2P_2O_7$ (a, c, e, g) and $Mn_3(PO_4)_2$ (b, d, f, h).

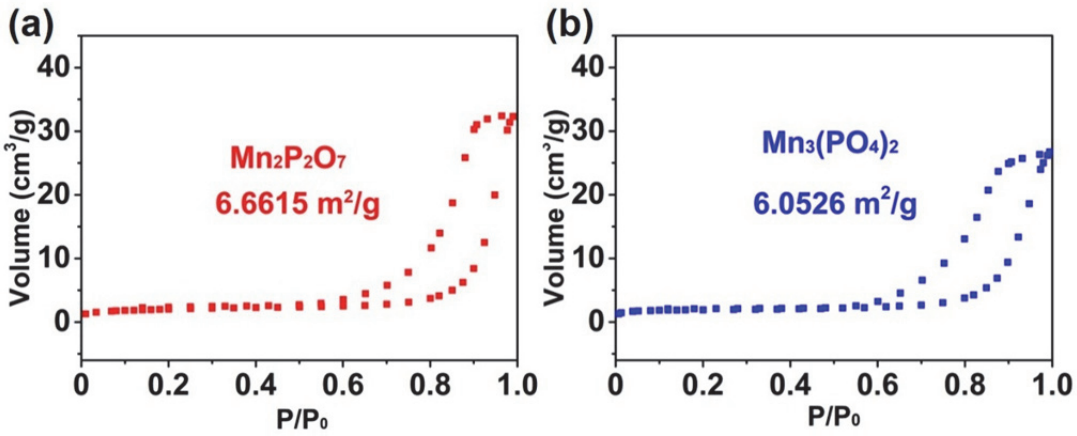

Fig S5. The nitrogen adsorption-desorption curves of (a) $Mn_2P_2O_7$ and (b) $Mn_3(PO_4)_2$.

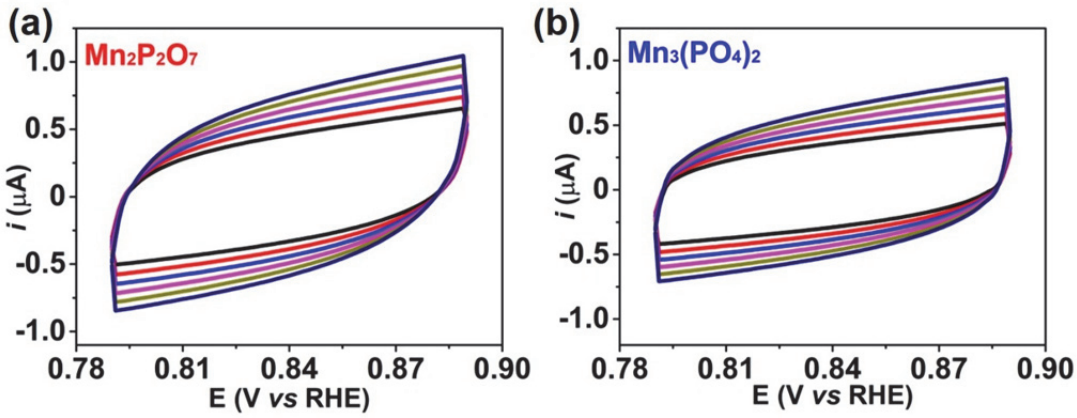

Fig S6. The charge and discharge currents of (a) $Mn_2P_2O_7$ and (b) $Mn_3(PO_4)_2$ measured in the non-Faradaic potential cover range with scan rates of 100, 120, 140, 160, 180 and 200 mV/s.

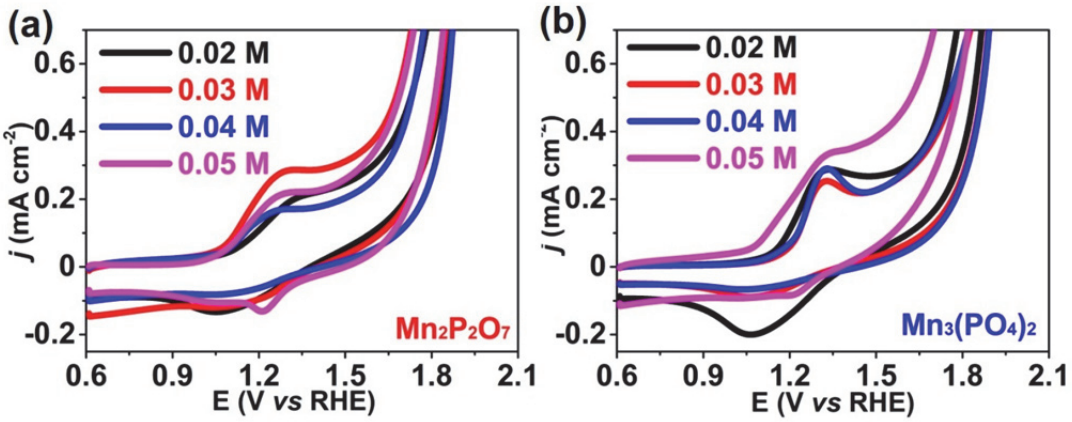

Fig S7. The current and potential response of the (a) $Mn_2P_2O_7$and (b) $Mn_3(PO_4)_2$ electrocatalyst to the concentration of phosphate anions.

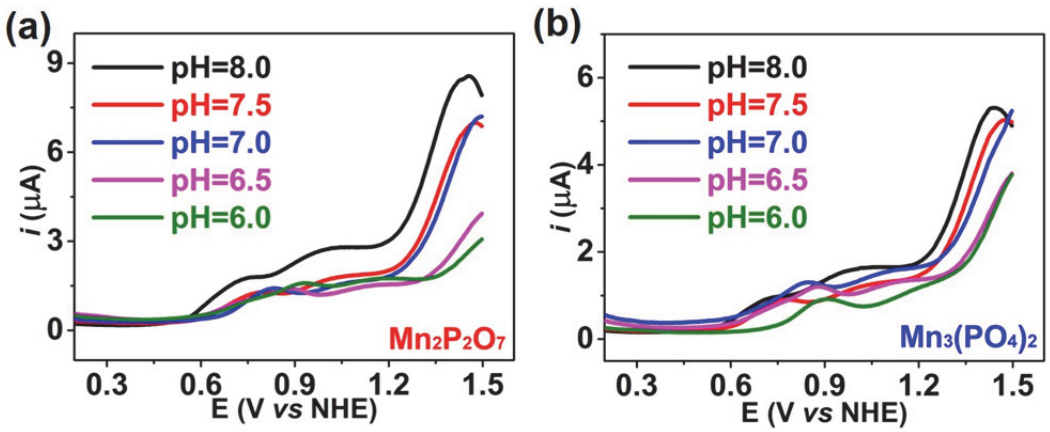

Fig S8. The kinetic currents and precatalytic oxidation potentials on pH value of electrolytes.

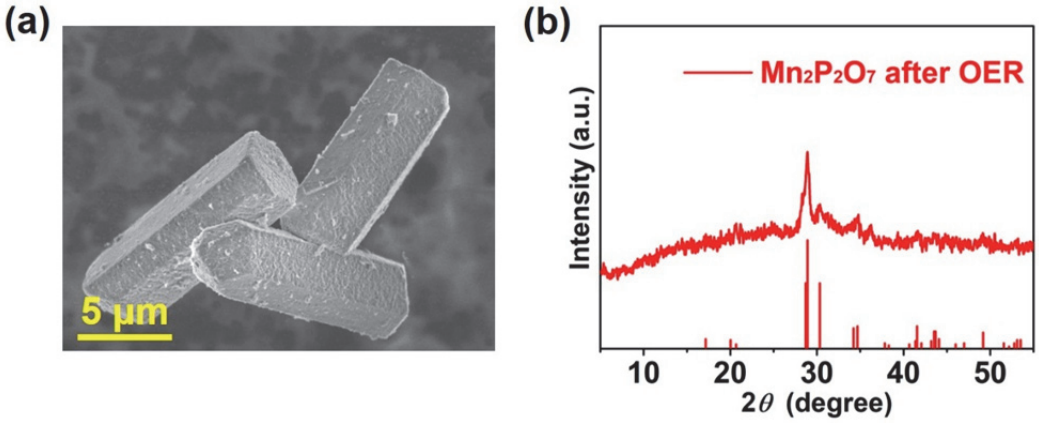

Fig. S9. The SEM image and XRD pattern of $Mn_2P_2O_7$ after OER stability test.

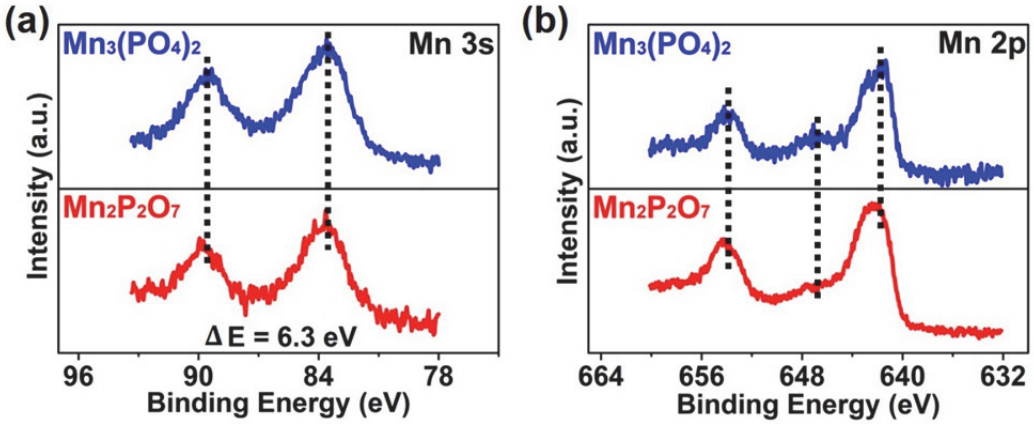

Fig S10. The Mn XPS spectra of $Mn_2P_2O_7$ (red) and $Mn_3(PO_4)_2$ (blue) after electrolysis.

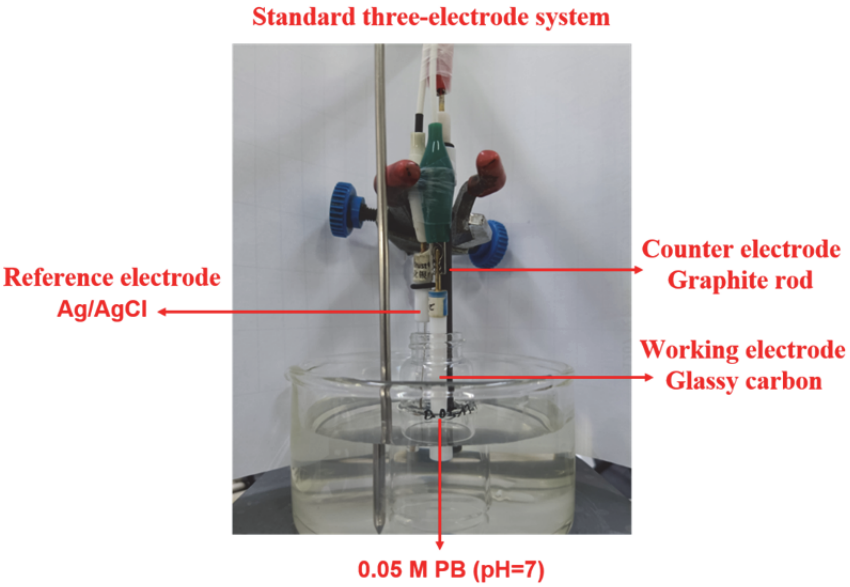

Fig S11. The electrochemical test equipment.

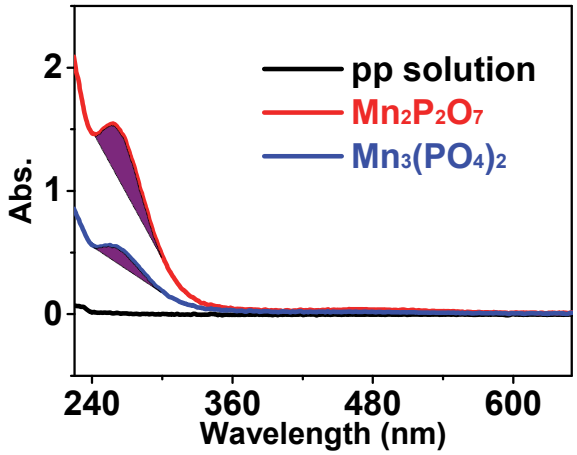

Fig S12. The UV-vis absorption peak area of the pyrophosphate (pp) solution after 2 h electrolysis.

References

1 G. Kresse, J. Furthmüller, *Computational materials science,* 1996, **6**, 15–50.

2 T. Bucko, J. Hafner, S. Lebegue, J. G. Angyán, *The Journal of Physical Chemistry A,* 2010, **114**, 11814–11824.

3 B. Hammer, L. B. Hansen, J. K. Nørskov, *Physical review B,* 1999, **59**, 7413.

4 J. P. Perdew, K. Burke, M. Ernzerhof, *Physical review letters,* 1996, **77**, 3865.

5 G. Kresse, D. Joubert, *Physical review b*, 1999, **59**, 1758.

6 P. E. Blöchl, O. Jepsen, O. K. Andersen, *Physical Review B*, 1994, **49**, 16223.

7 S. Grimme, S. Ehrlich, L. Goerigk, *Journal of computational chemistry,* 2011, **32**, 1456–1465.